

# Microstructure and Crystallographic Texture of Strip-Cast and Hot-Rolled Austenitic Stainless Steel

D. RAABE

The microstructure and texture of a strip-cast as well as a hot-rolled austenitic stainless steel (18 pct Cr, 8.5 pct Ni) are investigated by the use of optical metallography and quantitative X-ray texture analysis. In the hot band, a homogeneous microstructure is revealed together with a through-thickness texture gradient consisting of a weak cold rolling type of texture in the center layer and a shear texture close to the surface layers. The result is discussed in terms of the through-thickness shear profile that is generated during hot rolling. In the strip-cast material, a random orientation distribution as well as the development of martensite close to the center layer is attributed to the impingement and deformation of the films that are solidified on the surfaces of the casting rolls. The texture close to the surface is attributed to the growth selection of  $\{001\}\langle uvw \rangle$  oriented grains.

## I. INTRODUCTION

FLAT products of austenitic stainless steels are conventionally manufactured by continuous casting, hot rolling, subsequent cold rolling, and final recrystallization. Recent progress in strip-casting technology,<sup>[1,2]</sup> however, provides three main improvements in comparison to the customary processing method. First, it supplies an austenitic steel band with the same thickness and width as that which is produced by hot rolling. This permits the entire hot-rolling process to be bypassed. Second, the weak initial crystallographic texture of the strip-cast steel, which predetermines the deep drawing properties and strength of the final sheet as well as its weak through-thickness texture gradient, is responsible for a more homogeneous behavior when compared to hot-rolled sheets.<sup>[3,4]</sup> Third, it is not economical to produce small amounts of highly alloyed stainless steels by continuous casting and hot rolling. Strip casting is therefore likely to be a competitive method in the production of stainless steel sheets.

Whereas the texture and microstructure of cold rolled and recrystallized austenitic stainless steels have already been subject to detailed investigations in the past (*e.g.*, References 5 and 6), the corresponding microstructural features resulting from the recently introduced strip-casting technology as well as from the hot-rolling process have not yet been discussed in the literature. In the present work, therefore, the microstructure and crystallographic texture of a strip-cast sample were compared to those of a continuously cast and subsequently hot-rolled specimen. Both types of samples had a chromium (Cr) content of 18 wt pct and a nickel (Ni) content of 8.5 wt pct (Table I). The microstructure and texture were measured with high local resolution through the sheet thickness of both materials.

## II. EXPERIMENTAL PROCEDURE AND MEASUREMENT OF CRYSTALLOGRAPHIC TEXTURES

### A. Processing of the Samples

The hot rolling of the austenitic stainless steel (Table I) was industrially carried out after continuous casting, slab reheating, and initial reversing hot rolling in a conventional hot-strip mill, where the band is unidirectionally deformed in seven subsequent rolling passes. The temperature was between 1420 and 1470 K during the first hot-rolling pass and between 1050 and 1200 K during the last pass. The thickness of the hot band was 2.2 mm.

The austenitic strip cast samples (Table I) were industrially produced by casting liquid steel into a preheated tundish, which contacts two rotating, water-cooled steel rolls. The two casting rolls with different diameters are located in an "eleven o'clock position." The steel solidifies as a thin film on the roll surfaces. The process is controlled in such a way that the contact length between the liquid metal and the roll surface is equal for both rolls. In the roll gap, the films impinge and are compressed into a strip that leaves the gap with a temperature of about 1370 K.<sup>[1,2]</sup> The thickness of the strip cast sample was 2.4 mm. Both types of specimen were heat treated at 1370 K for 20 minutes and subsequently decaled.

Because the texture and microstructure of stainless steels are often inhomogeneous through the thickness,<sup>[7]</sup> the samples were inspected in various layers. In order to indicate the inspected layer, the parameter  $s = a/(1/2 \cdot d)$  is defined, where  $a$  is the distance from the center layer and  $d$  is the thickness of the sheet, *i.e.*, the surface layer is defined by  $s = 1$  and the center layer by  $s = 0$ . The textures of both types of samples were inspected in  $\Delta s = 0.1$  steps.

To remove a surface layer of 20  $\mu\text{m}$ , that is, to get rid of disturbing grinding effects before the texture

D. RAABE, Group Head, Research Group "Computer Simulation," is with the Institut für Metallkunde und Metallphysik, RWTH Aachen, 52056 Aachen, Germany.

Manuscript submitted June 9, 1994.

**Table I. Chemical Composition of the Austenitic Stainless Steel in Weight Percent**

C	Si	Mn	Cr	Mo	Ni	Fe
0.05	0.76	1.37	18.10	0.24	8.54	balance

measurements, the samples were etched in a solution of 100 ml H<sub>2</sub>O, 100 ml HCl, and 30 ml HNO<sub>3</sub> at a temperature of 330 K.

### B. Texture Measurement and Calculation

The crystallographic textures were quantitatively examined by measuring four incomplete {111}, {200}, {220}, and {113} pole figures by use of Mo<sub>Kα1</sub> radiation in the back-reflection mode.<sup>[8]</sup> From the pole figures, which are two-dimensional projections of the texture the three-dimensional orientation distribution function (ODF) was calculated by use of the series-expansion method.<sup>[9]</sup> In the case of cubic crystal symmetry and orthorhombic sample symmetry, which is set up by the rolling direction (RD), normal direction (ND), and transverse direction (TD), an orientation is represented by the three Euler angles  $\varphi_1$ ,  $\phi$ , and  $\varphi_2$  in the reduced Euler space. For better transparency, an orientation is often presented in terms of the Miller indices {hkl} <uvw>, where {hkl} describes the crystallographic plane which is parallel to the sheet surface and <uvw> the crystal direction that is parallel to RD.

Because austenitic steels tend to develop characteristic fiber textures during rolling,<sup>[5,6]</sup> it is convenient to depict the ODFs as isointensity diagrams in  $\varphi_2$  sections through Euler space. In Figure 1, the most relevant fibers and orientations are displayed schematically.

- $\alpha$  fiber: <110> || ND, main orientations: {011}<100>, {011}<2-11>, {011}<1-11>, and {011}<0-11>.
- $\gamma$  fiber: {111} || ND, main orientations: {111}<0-11> and {111}<-1-12>.
- $\tau$  fiber: <110> || TD, main orientations: {001}<1-10>, {112}<-1-11>, {111}<-1-12>, and {011}<100>.
- $\beta$  fiber: less-symmetric-texture fiber containing the orientations: {11-2}<111> (C), {123}<-6-34> (S), and {011}<2-11> (B).

## III. EXPERIMENTAL RESULTS

### A. Microstructure

As can be seen in the longitudinal section, the hot-rolled material displays a homogeneous microstructure through the thickness of the sheet (Figure 2). Many twin boundaries can be seen in all layers. Basically, the microstructure is more homogeneous than that of the hot-rolled ferritic stainless steels.<sup>[7]</sup>

In the longitudinal section of the strip-cast steel (Figure 3), a more inhomogeneous microstructure through the thickness of the sheet is detected when compared to the hot-rolled material (Figure 2). Whereas large, uniformly oriented blocks of austenitic dendrites can be seen (Figure 4(a)) between the surface and the near-center

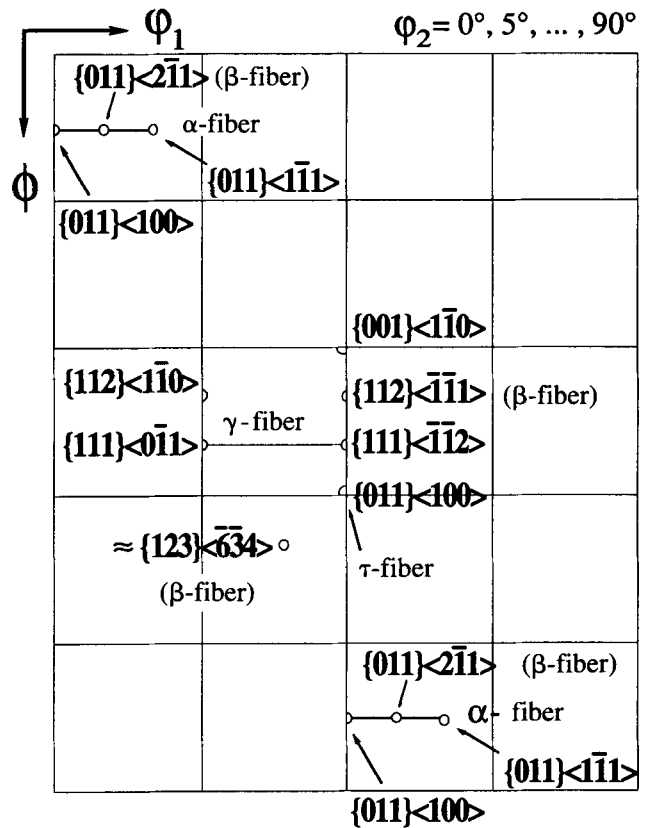


Fig. 1—Some relevant orientations and texture fibers that occur in strip-cast and hot-rolled austenitic stainless steels.

layers, *i.e.*, between  $s = 1$  and  $s \approx 0.4$ , close to the center layers, a different microstructure appears. Between  $s \approx 0.3$  and 0.1, a more blocky and nearly equiaxed morphology of the austenite has developed, which contains some martensite plates (Figure 4(b)). Between  $s \approx 0.1$  and 0, *i.e.*, in the center of the material, a globular austenitic grain structure with a martensitic volume fraction of up to 20 pct becomes visible (Figure 4(b)). In contrast to this finding, the course of the microhardness (100 g Vickers), however, does not reveal an enhanced value close to the center layer (Figure 5).

### B. Crystallographic Texture

The hot band reveals an inhomogeneous texture profile through the thickness of the sheet. Close to the center layer, *i.e.*, at  $s = 0.0$  and 0.1, the orientation distribution is characterized by a weak  $\beta$  fiber with a maximum at {011}<211> (Figure 6(a)). A continuous  $\alpha$  fiber does not occur (Figure 7(a)). A second important feature of the texture at  $s = 0.0$  is the appearance of the cube component {001}<100> (Figures 6(a) and 8(a) through (c)). In the  $s = 0.2$  layer, the previously mentioned orientations are completely decreased and a nearly random orientation distribution is revealed (Figures 6(b) and 7(b)). Close to the  $s = 0.5$  and  $s = 0.6$  layers, a texture transition takes place (Figure 6(c)). First, a weak {001}<110> component (Figures 8(a) through (c) and 6(c)), second, a  $\gamma$  fiber (Figures 8(d) and 6(c)) and third, a strong {112}<110> orientation is generated



Fig. 2—Longitudinal section, not-rolled austenitic steel.

(Figure 6(c)), which corresponds to the 30 deg about TD rotated rolling component  $\{110\}\langle 112 \rangle$ . In the subsurface layers ( $s = 0.7$  to  $0.8$ ), the orientation distribution is again randomized (Figures 6(d), 7, and 8). At the surface ( $s = 1.0$ ), a similar texture as in layer  $s = 0.6$  is developed (Figure 6(c)). To describe the shear texture profile through the thickness of the hot-rolled sheet, two relevant texture components, namely  $\{001\}\langle 110 \rangle$  and the

maximum close to  $\{111\}\langle 110 \rangle$ , are employed (Figure 9). It is revealed that the orientation densities of both components display similar profiles through the thickness of the sheet. Close to the center layers, both orientations are weak and increase continuously in intensity up to the

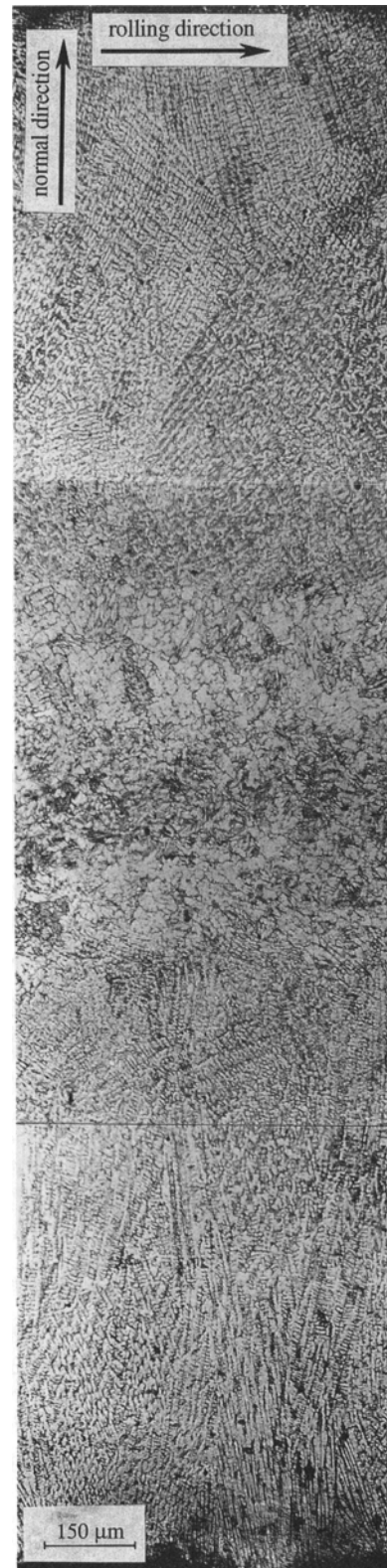


Fig. 3—Longitudinal section, strip-cast austenitic steel.

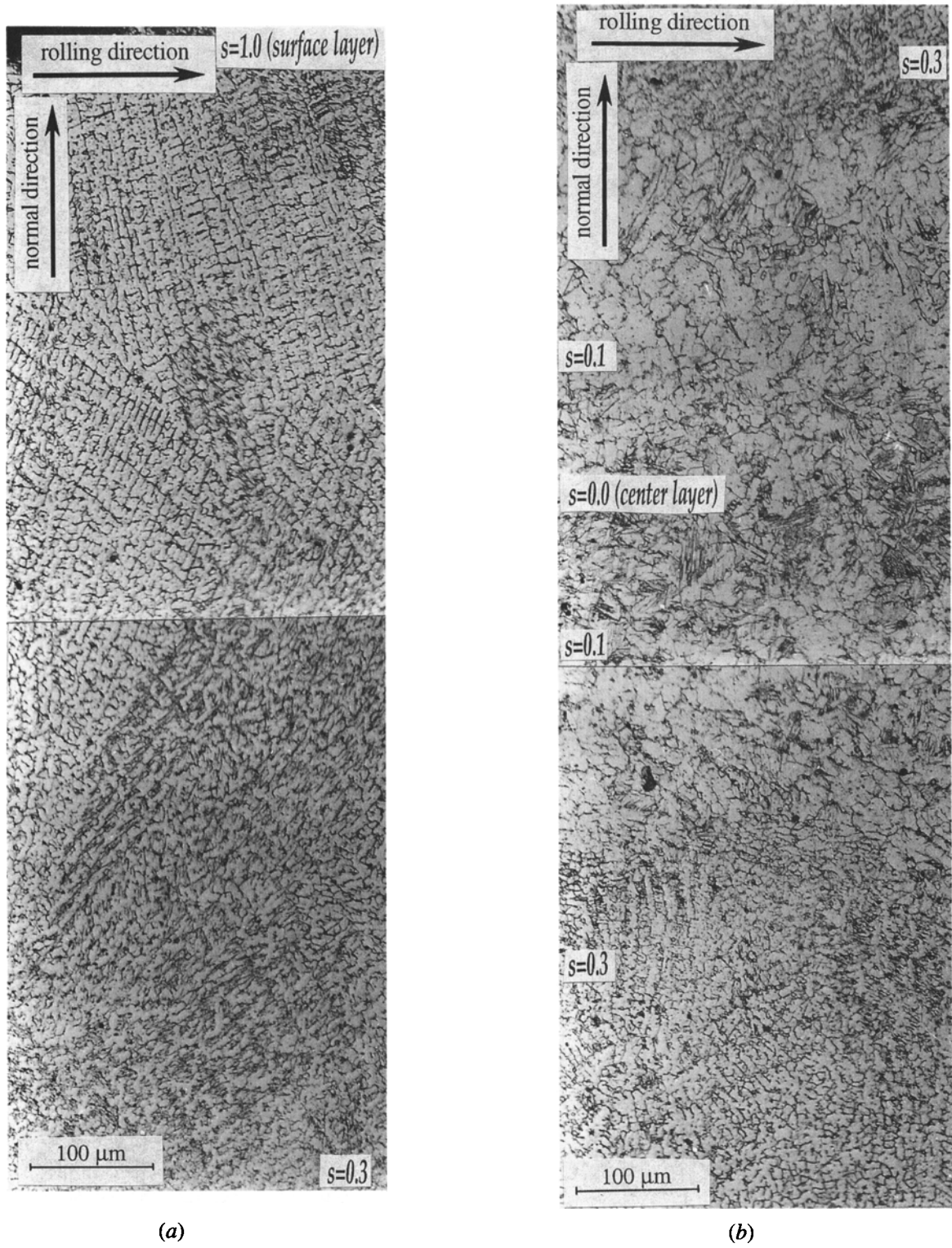


Fig. 4—Longitudinal section, strip-cast austenitic steel: (a) near-surface layers and (b) center layers.

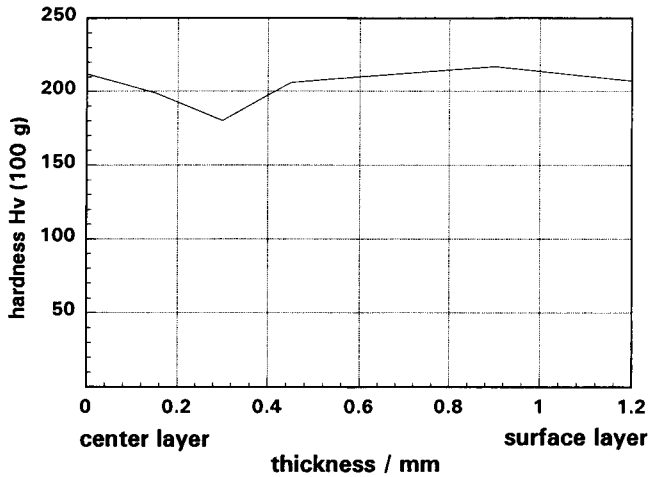


Fig. 5—Profile of microhardness through the thickness of the strip-cast sample.

$s = 0.6$  layer. Between  $s = 0.6$  and  $0.9$ , a decrease and, at the surface again, an enhancement can be seen.

In the strip-cast material, also, different types of textures occur in the center and in the surface layers. The texture gradients observed here are, however, less pronounced than in the hot-rolled steel. Close to the center of the cast band ( $s = 0.0$  to  $s = 0.3$ ), a random texture with orientation densities below 2.3 is detected (Figure 10). Between  $s \approx 0.4$  (Figure 10(b)) and the surface layer,  $s = 1.0$  (Figure 10(c)), a weak fiber texture close to  $\{001\}\langle uvw \rangle$  is generated. From the first occurrence of this fiber at  $s \approx 0.3$  and  $0.4$ , the orientation density increases from  $f(g) = 2.4$  up to  $f(g) = 4$  at  $s = 1.0$ .

#### IV. EVALUATION OF THE RESULTS

##### A. Hot Rolling

The most striking feature of the hot-band texture is the occurrence and profile of the through-thickness inhomogeneity. This is characterized by a weak  $\beta$  fiber

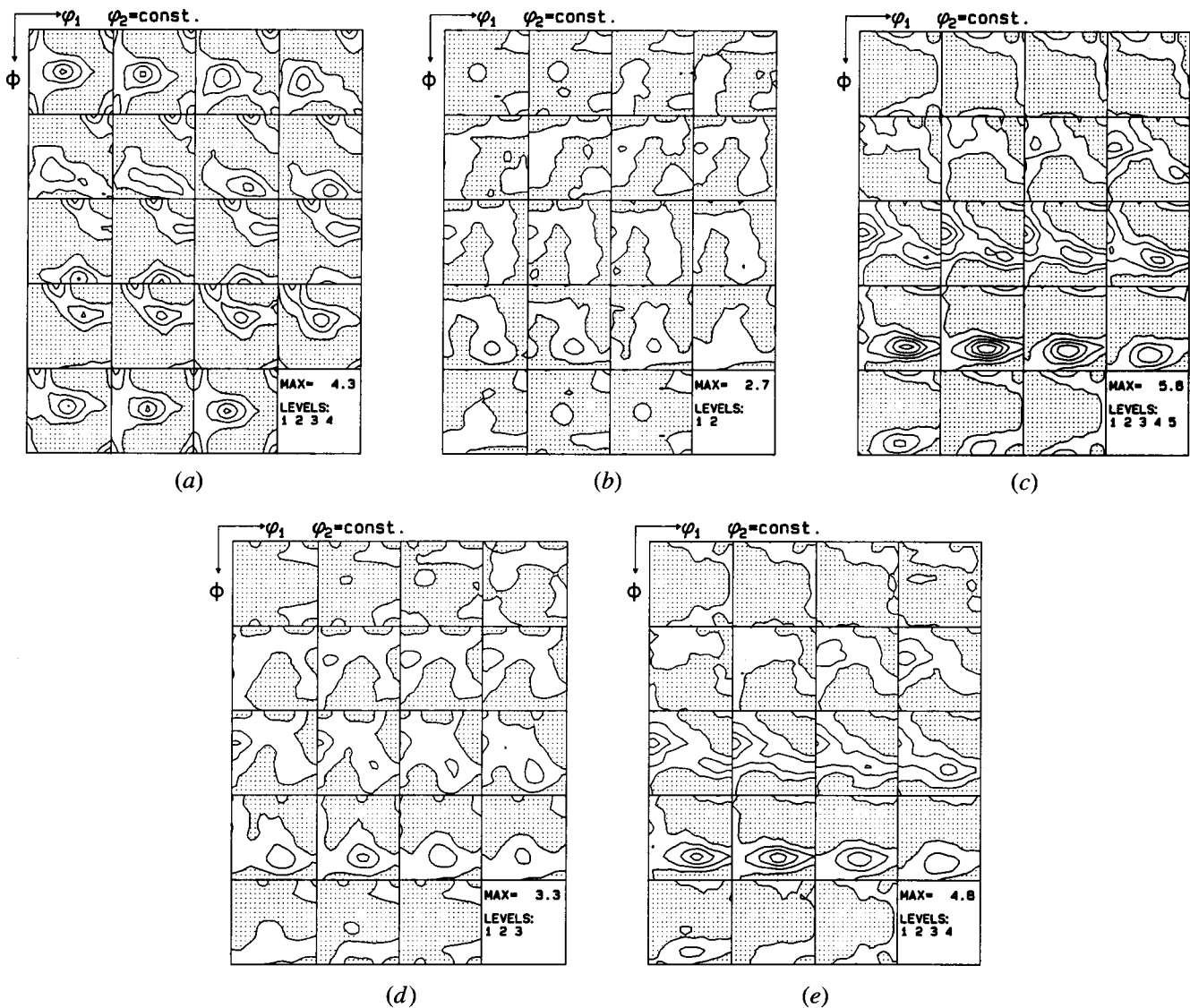


Fig. 6—Orientation distribution in the hot-rolled steel and various through-thickness layers: (a)  $s = 0$  (center layer), (b)  $s = 0.2$ , (c)  $s = 0.6$ , (d)  $s = 0.7$  and (e)  $s = 1.0$  (surface layer).

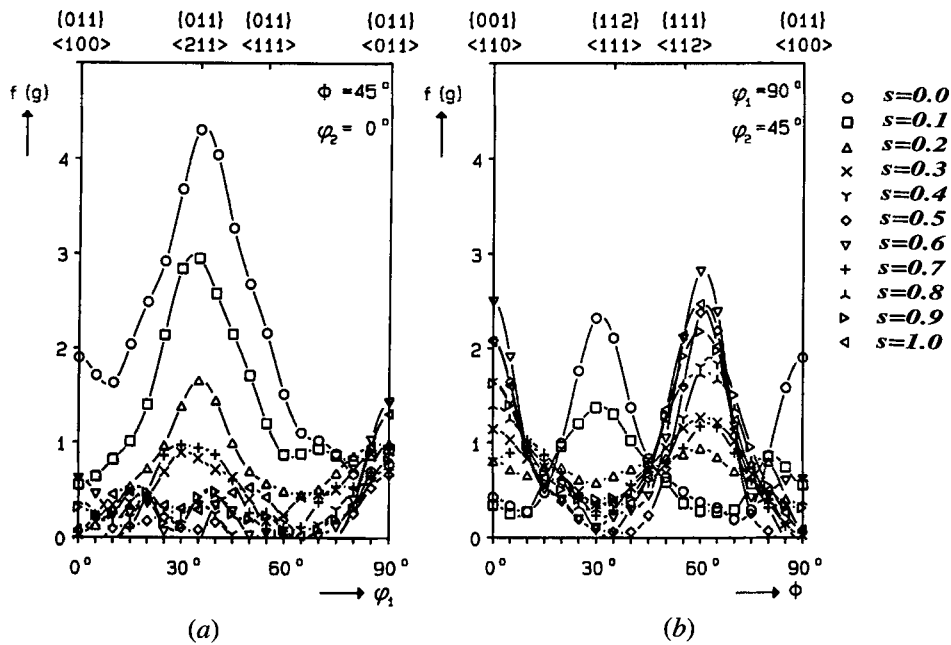


Fig. 7—Orientation distribution in the hot-rolled steel and 11 various through-thickness layers, fiber presentation: (a)  $\alpha$  fiber and (b)  $\tau$  fiber.

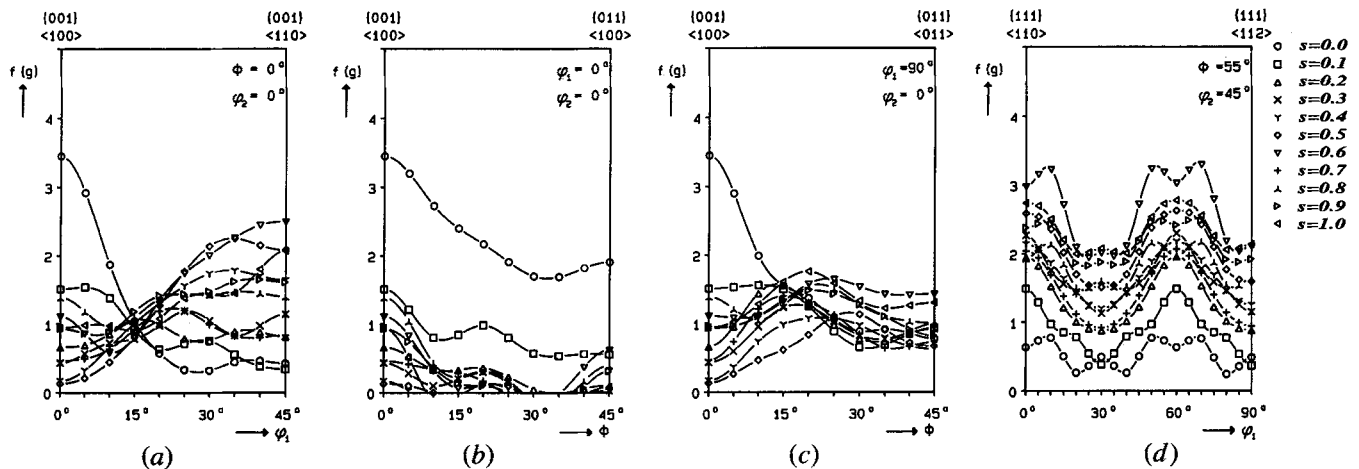


Fig. 8—Orientation distribution in the hot-rolled steel and 11 various through-thickness layers, fiber presentation: (a) rotations of the cube component about normal direction, (b) rotations of the cube component about rolling direction, (c) rotations of the cube component about transverse direction, and (d)  $\{111\}$  fiber.

accompanied by the cube orientation in the center layer (Figure 6(a)) and by a  $\gamma$  fiber, the rotated cube orientation and the  $\{112\}\{110\}$  component close to the surface layers (Figures 6(c) and (e)). As depicted in Figure 9, two maxima of the orientation density of the latter type of texture occur, one at  $s \approx 0.6$  and another one at  $s = 1.0$ .

In accordance with numerous experimental results by Goodman and Hu<sup>[5]</sup> and Donadille *et al.*,<sup>[6]</sup> as well as Taylor type simulations by Hirsch *et al.*,<sup>[10]</sup> the observed  $\beta$  fiber at  $s = 0$  (Figure 6(a)) is a typical texture, which is generated during the plane strain rolling deformation of face-centered cubic (fcc) polycrystals at ambient temperatures.<sup>[5,6,10]</sup> However, in the present case, the maximum orientation density is much lower than after cold rolling. Because complete recrystallization during or after

hot rolling would have removed the detected rolling texture at  $s = 0$ , this result suggests that a high volume fraction of the material has merely undergone recovery. This finding, however, contradicts two other facts. First, the microstructure (Figure 2) reveals a fairly equiaxed instead of an elongated, recovered grain morphology. Second, the stacking fault energy (SFE) of the present austenitic stainless steels is very low, namely  $21 \cdot 10^{-3} \text{ J/m}^2$ .<sup>[11]</sup> The corresponding normalized value, *i.e.*, the SFE divided by the Burgers vector and the shear modulus is equal to  $0.68 \cdot 10^{-3}$ , which is of the order of the value for 70/30 brass. This fact implies that a strong tendency for recrystallization instead for recovery can be expected.

It thus seems more likely that recrystallization has renewed the microstructure during the first hot-rolling passes

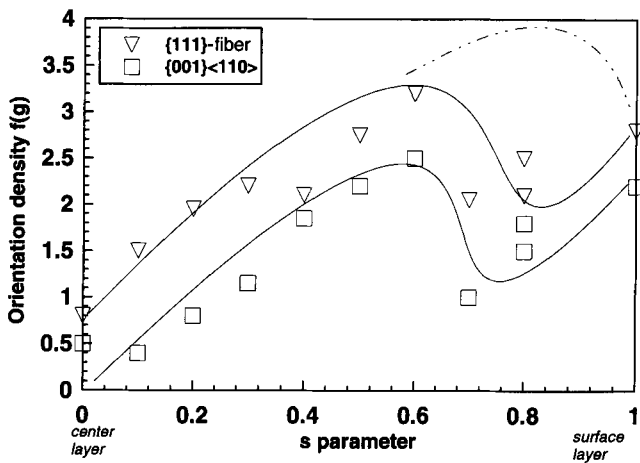


Fig. 9—Profile of the orientation density of the  $\{001\}\langle 110 \rangle$  orientation and of the maximum of the  $\{111\}$  fiber through the thickness of the hot-rolled sample (dotted line: schematically presented profile of the through-thickness shear according to Refs. 17 and 18 for the industrial hot rolling of stainless steel).

and that the weak  $\beta$  fiber texture was developed only during the last one or two rolling passes. In this regime, the sheet has undergone considerable cooling, *i.e.*, the temperature of the band and the stored energy imposed by the last rolling pass were too low for recrystallization. This conclusion is in good accordance with the low observed orientation density of 4.3, since the steady recovery of rolled material would have led to a much stronger texture maximum.

A second relevant feature of the center layer texture of the hot band is the occurrence of the cube orientation (Figure 5(a)). This component has also been found in the center layers of hot-worked aluminum.<sup>[12]</sup> According to Le Hazif *et al.*<sup>[13]</sup> and Maurice and Driver,<sup>[14]</sup> who have carried out slip-line investigations on hot-rolled aluminum, this texture component results from the activation of dislocation glide on  $\{110\}\langle 110 \rangle$  in addition to

$\{111\}\langle 110 \rangle$  slip systems at homologous rolling temperatures above 0.6. Due to the low SFE of the austenite, however, it is more likely that the cube component results from recrystallization than from deformation, since the grains in the hot band reveal an equiaxed and not an elongated morphology (Figure 2).

The textures in the other layers reveal distinct differences to the orientation distribution at  $s = 0$ . Whereas in some layers a random texture occurs (Figures 6(b) and (d)), at  $s = 0.6$  (Figures 6(c), 8, and 9) and  $s = 1$  (Figures 6(e), 8, and 9), a  $\gamma$  fiber accompanied by a  $\{001\}\langle 110 \rangle$  and a  $\{112\}\langle 110 \rangle$  orientation is detected. All three texture components are well known from inhomogeneously rolled aluminum and represent typical orientations that are generated by strong shear deformation.<sup>[12,15,16]</sup> According to Mao, the present  $\{112\}\langle 110 \rangle$  component results from the  $\{011\}\langle 211 \rangle$  orientation, which represents the strongest plane strain rolling component in low SFE fcc metals<sup>[10]</sup> and which has been rotated 30 deg about the TD due to the rotation of the strain state.<sup>[16]</sup> A similar through-thickness profile of the comparative shear orientations is also well investigated for hot-rolled ferritic stainless steels.<sup>[7]</sup> Whereas in these works,<sup>[7,12,15,16]</sup> however, the strongest shear and thus also the highest orientation densities of the corresponding texture components occur at  $s = 0.7$  to 0.8, in the present austenitic hot band the maximum of the shear texture is locally split into one peak at  $s = 0.6$  and a second one at  $s = 1$ . At  $s = 0.7$  to 0.8 even a local minimum of the relevant texture components can be seen (Figure 9). Although the observed orientation densities are very weak, this effect is in clear contradiction to the experimentally detected<sup>[7,12,15]</sup> and especially to the calculated shear profiles that have been reported by Beynon *et al.*<sup>[17]</sup> and McLaren and Sellars<sup>[18]</sup> for the industrial hot rolling of stainless steels.

In order to interpret the texture profile here observed, it is thus suggested that the expected maximum of shear was indeed situated in the range between  $s = 0.7$  and

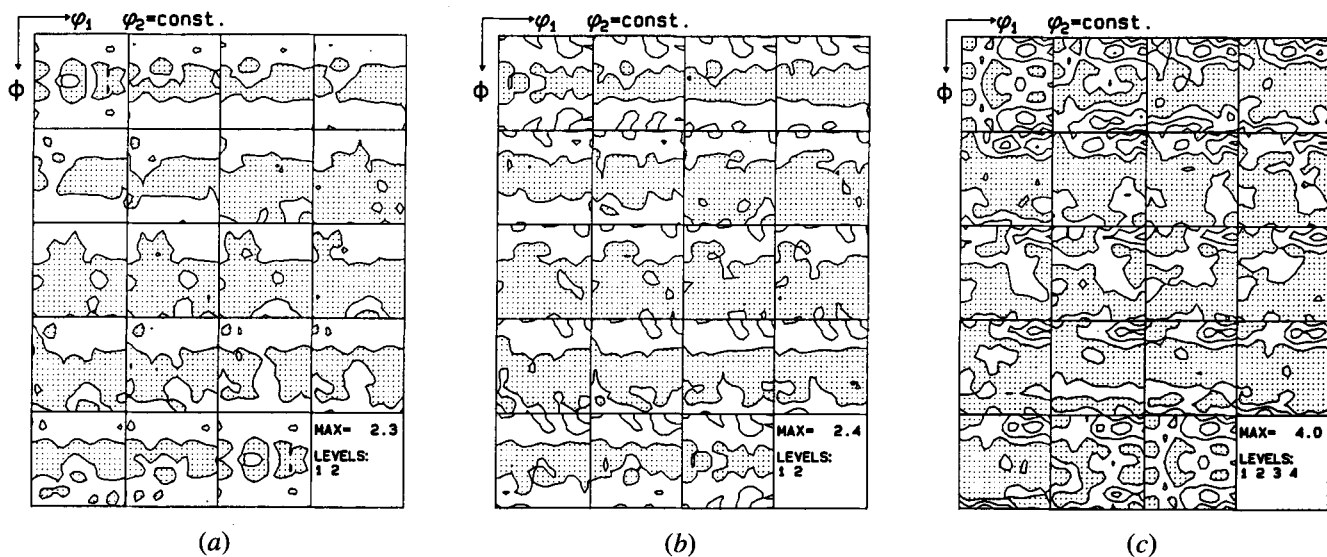


Fig. 10—Orientation distribution in the strip-cast steel and various through-thickness layers: (a)  $s = 0.2$  (near-center layer), (b)  $s = 0.4$ , (c)  $s = 1.0$  (surface layer).

0.8, as predicted by simulations<sup>[17,18]</sup> and as schematically marked by the dotted line in Figure 9. But since this implies a higher local deformation at that depth, *i.e.*, a higher stored dislocation energy, recrystallization can easily have taken place in these layers, leading to the randomization of the texture.

The observed texture profile which is—in accordance with simulations and experiments<sup>[7,15-18]</sup>—thus mainly attributed to the through-thickness profile of the shear during the last one or two hot-rolling passes, relates only weakly to the homogeneous through-thickness microstructure. This result corresponds to findings in hot bands of ferritic stainless steel.<sup>[7]</sup>

## B. Strip Casting

In the strip-cast material, two types of textures can be detected through the sheet thickness: first, a random texture in the center layers ( $s = 0.0$  to  $0.3$ ) (Figure 10(a)), and second, an orientation fiber that is characterized by  $\{001\}\langle uvw \rangle$  between  $s \approx 0.4$  and  $s = 1.0$  (Figure 10(c)). In contrast to the orientation distribution in the hot band, in the strip-cast steel, both types of textures are locally related to optically visible features of the microstructure (Figures 3 and 4).

The random texture between  $s = 0.0$  and  $s \approx 0.3$  corresponds to a globular morphology of the austenite, which contains small volume fractions of cubic martensite (Figure 4(b)). It can be seen that the microstructure in the near-surface layers is not deformed or bent but appears as large blocks of austenitic dendrites (Figure 4(a)). The austenitic alloy investigated here tends to form cubic martensite under the influence of deformation (which usually happens during cold rolling and not during hot processing). This means that the hot deformation that occurs during impingement of the two solidified steel films has caused the observed equiaxed microstructure, the deformation induced martensite, and the randomization of the texture.

Because a  $\{001\}\langle uvw \rangle$  texture is detected closer to the surface layers, growth selection during solidification of the austenitic dendrites, which were formed on the surfaces of the casting rolls, may be assumed. Also, from the solidification of aluminium, the occurrence of a crystallographic texture fiber with a  $\langle 100 \rangle$  direction parallel to ND has been reported.<sup>[19]</sup>

## V. SUMMARY AND CONCLUSIONS

The development of microstructure and texture has been investigated in a strip cast as well as in a hot-rolled austenitic stainless steel with 18 pct Cr and 8.5 pct Ni. The hot band revealed a weak orientation distribution with a gradient between the center and surface layers. In the center of the sheet, a cold-rolling type of texture, *i.e.*, a  $\beta$  fiber accompanied by a cube orientation, was detected, which was not randomized by recrystallization. It was hence concluded that this texture was essentially

formed during the last hot-rolling passes. Close to the surface, a shear texture consisting of a  $\gamma$  fiber, a  $\{001\}\langle 110 \rangle$ , and a  $\{112\}\langle 110 \rangle$  component was detected, which corresponds to similar findings in hot-rolled aluminium. The absence of the maximum of the shear texture at  $s = 0.7$  to  $0.8$  was explained by recrystallization.

In the strip-cast specimen, the random orientation distribution as well as the occurrence of martensite close to the center layer were attributed to the impingement and deformation of the films that were solidified on the surfaces of the casting rolls. The texture close to the surface was attributed to the growth selection of  $\{001\}\langle uvw \rangle$  oriented grains.

## ACKNOWLEDGMENTS

The author gratefully acknowledges the kind support by the strip-casting research group of Krupp-Hoesch Stahl AG, especially of Drs. M. Dubke and M. Hölscher.

## REFERENCES

1. K. Ohno, H. Tanaka, T. Sasaki, M. Dubke, H.J. Funk, K.H. Hanke, H. Pfeifer, and R. Hentrich: *Proc. Int. Conf. on New Smelting Reduction and Near Net Shape Casting Technologies for Steel*, Pohang, Korea, Korean Institute of Metals, 1990, pp. 14-22.
2. R. Hentrich, M. Dubke, H.J. Funk, K.H. Hanke, J. Loh, and S. Kuhlmann: *Stahl Eisen*, 1991, vol. 111, pp. 51-55.
3. D. Raabe, M. Hölscher, M. Dubke, H. Pfeifer, K.H. Hanke, and K. Lücke: *Steel Res.*, 1993, vol. 64, pp. 359-63.
4. D. Raabe, M. Hölscher, M. Dubke, and K. Lücke: *Proc. Int. Conf. on Strip Casting, Hot and Cold Working of Stainless Steels*, PQ, Canada, Aug. 29–Sept. 2, 1993, Quebec, Canada, N.D. Ryan, A.J. Brown, and H.J. McQueen, eds., The Metallurgical Society of CIM, PQ, Canada, 1993, pp. 3-17.
5. S.R. Goodman and H. Hu: *Trans. AIME*, 1964, vol. 230, pp. 1413-21.
6. C. Donadille, R. Valle, P. Dervin, and R. Penelle: *Acta Metall.*, 1989, vol. 37, pp. 1547-71.
7. D. Raabe and K. Lücke: *Mater. Sci. Technol.*, 1993, vol. 9, pp. 302-12.
8. L.G. Schulz: *J. Appl. Phys.*, 1949, vol. 20, pp. 1030-34.
9. H.J. Bunge: *Z. Metallkd.*, 1965, vol. 56, pp. 872-74.
10. J. Hirsch and K. Lücke: *Acta Metall.*, 1988, vol. 36, pp. 2863-2927.
11. R.E. Schramm and R.P. Reed: *Metall. Trans. A*, 1975, vol. 6A, pp. 1345-51.
12. J. Hirsch: *Hot Deformation of Aluminium Alloys*, T.G. Langdon, M.D. Merchant, J.G. Morris, and M.A. Zaidi, eds., TMS, Warrendale, PA, 1991, pp. 379-85.
13. R. Le Hazif, P. Dorizzi, and J.P. Poirier: *Acta Metall.*, 1973, vol. 21, pp. 903-11.
14. Cl. Maurice and J.H. Driver: *Acta Metall.*, 1993, vol. 41, pp. 1653-64.
15. M. Hölscher, D. Raabe, and K. Lücke: *Acta Metall.*, 1994, vol. 42, pp. 879-86.
16. W. Mao: Doctoral Thesis, RWTH Aachen, 1988, pp. III-11-19 and III-28.
17. J.H. Beynon, P.R. Brown, S.I. Mizban, A.R.S. Ponter, and C.M. Sellars: in *Computational Methods for Predicting Material Processing Defects*, M. Predeleanu, ed., Elsevier, Amsterdam, 1987, pp. 19-28.
18. A.J. McLaren and C.M. Sellars: *Mater. Sci. Technol.*, 1992, vol. 8, pp. 1090-94.
19. J. Hirsch, E. Nes, and K. Lücke: *Acta Metall.* 1987, vol. 35, pp. 427-38.